Supporting Information for

In-Situ Etch Engineering Ru Doped $NiFe(OH)_x$/NiFe-MOF Nanocomposite for Boosting Oxygen Evolution Reaction

Dongmei Liu[a], Hui Xu[c], Cheng Wang[a], Changqing Ye[b]*, Rui Yu[a], Yukou Du[a]*

[a]*College of Chemistry, Chemical Engineering and Materials Science, Soochow University, 199 Renai Road, Suzhou 215123, P.R. China.*

[b]*Jiangsu Key Laboratory for Environmental Functional Materials, Institute of Chemistry, Biology and Materials Engineering, Suzhou University of Science and Technology, Suzhou 215009, PR China.*

[c]*Key Laboratory of Advanced Catalytic Materials and Technology, Advanced Catalysis and Green Manufacturing Collaborative Innovation Center, Jiangsu Key Laboratory of Oil and Gas Storage & Transportation Technology, Changzhou University, Jiangsu, 213164, China*

** Corresponding authors: Tel: 86-512-65880089, Fax: 86-512-65880089;*

E-mail: yechangqing@mail.usts.edu.cn (C. Ye); duyk@suda.edu.cn (Y. Du)

Experimental Sections

Synthesis of NH_2-MIL-101 (Fe)

The octahedral NH_2-MIL-101 (Fe) (denoted as Fe-MOF) was synthesized following the previously reported method. Typically, 1.24 mmol of NH_2-BDC (2-amino terephthalic acid) was dispersed in 15 mL DMF (N, N-dimethylformamide), then the

above mixture was added into a solution containing 2.5 mmol of $FeCl_3 \cdot 6H_2O$ and 15 mL DMF. After ultrasonic treatment for 30 min, the dark brown precipitate was transferred to a teflon-lined stainless-steel autoclave, subsequently heated from room temperature to 110°C and maintained at 110°C for 20 h. The resulting products were centrifuged and washed with DMF and ethanol for several times, then dried under vacuum for 12 h.

Synthesis of NiFe-MOF

Ni doped NH_2-MIL-101 (Fe) (marked as NiFe-MOF) was synthesized by a facile hydrothermal method. Typically, 30 mg of $NiCl_2 \cdot 6H_2O$ was dissolved in 15 mL of DMF, then the above solution was added to a mixture of 15 mL DMF and the as-prepared 20 mg NH_2-MIL-101 (Fe). After ultrasonic treatment for 30 min, the dark green precipitate was transferred to a teflon-lined stainless-steel autoclave, then heated from room temperature to 80°C and maintained at 80°C for 24 h. The resulting products were centrifuged and washed with DMF and ethanol for several times, then dried under vacuum for 12 h.

Synthesis of $NiFe(OH)_x$/NiFe-MOF

The $NiFe(OH)_x$/NiFe-MOF composite was prepared through an ammonia etching strategy. Firstly, 20 mg of the NiFe-MOF was dispersed into a solvent containing 9 mL deionized water and 9 mL ethanol. After ultrasonic treatment for 10 min, 2 mL of $NH_3 \cdot H_2O$ (25%~28%) was dropwise added into the above solution with constant stirring for 10 min till the color of the precipitate changed from dark brown to light

orange, the products were centrifuged and washed with deionized water and ethanol for several times, then dried under vacuum for 12 h. To explore the influence of etching time, we prepared a series of $NiFe(OH)_x$/NiFe-MOF with reaction time of 30 min and 1h under the same condition.

Synthesis of Ru/$NiFe(OH)_x$/NiFe-MOF

Ru doped $NiFe(OH)_x$/NiFe-MOF was synthesized by a facile ion exchange process, 4 mg $RuCl_3$ was added into 15 mg of the $NiFe(OH)_x$/NiFe-MOF in 15 mL ethanol, after magnetic stirring for 24 h, the resulted dark gray products were centrifuged and washed with deionized water and ethanol for several times, and then dried under vacuum for 12 h.

Synthesis of Ru@NiFe-MOF

Ru doped NiFe-MOF was synthesized by the similar ion exchange process. Breifly, 4 mg $RuCl_3$ was added into 15 mg of the NiFe-MOF in 15 mL ethanol, after magnetic stirring for 24 h, the resulted products were centrifuged and washed with deionized water and ethanol for several times, and then dried under vacuum for 12 h.

Characterization

Low-magnification transmission electron microscopy (TEM) was performed on a HITACHI HT7700 at 120 kV. High-angle annular dark-field scanning transmission electron microscopy (HAADF-STEM) and high-resolution TEM (HRTEM) was recorded on a FEI TecnaiG2F2 FEI Talos F200X S/TEM with a field-emission gun at 200 kV. The energy-dispersive X-ray (EDX) spectroscopy which combined with

scanning electron microscopy (SEM) was conducted on a Hitachi S-4700 instrument operated at 15 kV under high vacuum, UV/Visible diffuse reflectance spectra (UVDRS) of the powders was conducted on a UV-3600 Plus spectrophotometer (SHIMAZU, Japan). Fourier infrared spectrometer (FTIR, Bruker Vertex70, Germany) was used to determin the organic linker in MOFs structures, the wavelength was selected from 4000 to 600 cm^{-1}, and X-ray photoelectron spectroscopy (XPS) was performed on a VG scientific ESCA Lab 220 XL electron spectrometer using 300 W Al Kα radiation.

OER Electrochemical tests

All the electrochemical measurements were conducted on a CHI 660E electrochemical analyzer (Chenhua, Shanghai) in 1 M KOH electrolyte. To obtain the catalyst ink, 2.5 mg catalyst and 2.5 mg carbon powder were added into a mixture of 1 mL ethanol and 10 μL 5 wt% Nafion solution, after 20 min sonication, 10 μL of the as-obtained catalyst ink was deposited on the polished glassy carbon electrode (GCE) (diameter: 5 mm, area: 0.196 cm^2) which served as the working electrode. A graphite rod was performed as the counter electrode, and the saturated Ag/AgCl electrode was used as the reference electrode. All the reference potentials were transformed into the reversible hydrogen electrode (RHE) by the following formula: E_{RHE} = E (Ag/AgCl) + 0.059 × pH + 0.197 V,6 the overpotential (η) was calculated by $\eta = E_{RHE} - 1.23$ V. The polarization curves were measured by linear sweep voltammetry (LSV) at a rate of 5 mV s^{-1} with potential range from 1.0 V to 1.7 V (vs. RHE). The Tafel plots were figured out by the Tafel equation: $\eta = a + b \lg j$, where η is overpotential, j is the

current density, and b is the Tafel slope. Cyclic voltammetry (CV) curves were collected in non-faradic region (0.00 V - 0.10 V vs. Ag/AgCl) with scan rates of 5 mV s^{-1} to 50 mV s^{-1} in 1.0 M KOH. The electrochemical impedance spectroscopy (EIS) tests were carried out with the frequency ranging from 0.01 to 100 kHz. All the electrochemical tests were conducted without iR compensation.

Supporting Figures and Tables

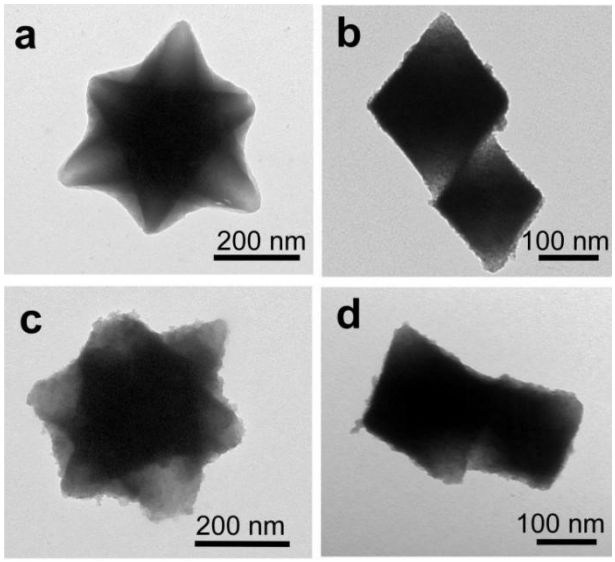

Fig.S1 (a, c) TEM images of Fe-MOF and NiFe-MOF observed from the top view. (b, d) TEM images of Fe-MOF and NiFe-MOF observed from the side view.

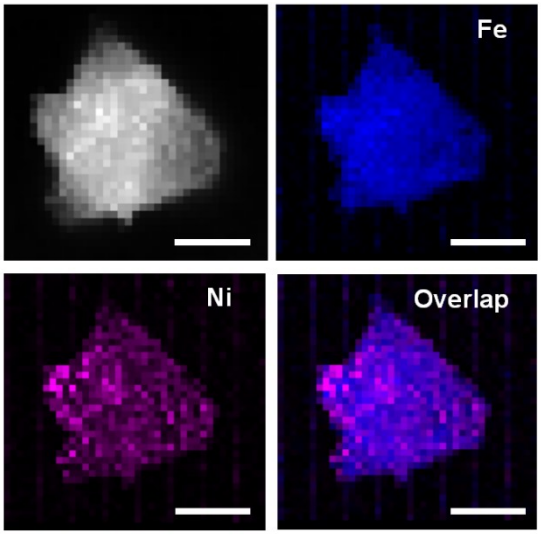

Fig.S2 HAADF-STEM and EDS element mapping images of NiFe-MOF. Scale bars are 100 nm.

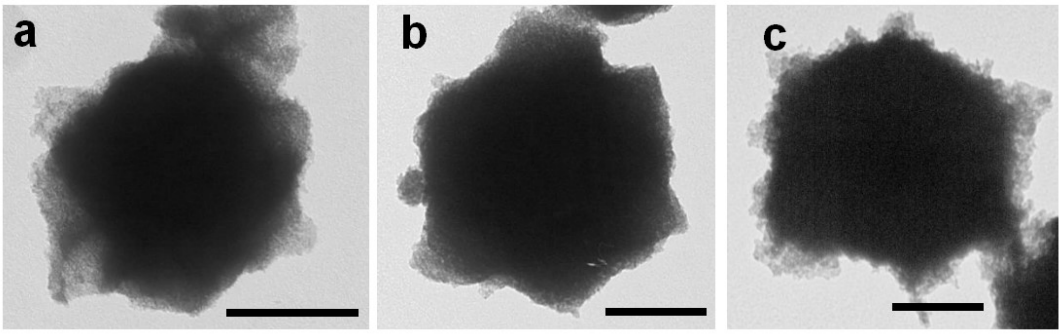

Fig.S3 TEM images of NiFe(OH)$_x$/NiFe-MOF etching for (a) 10 min, (b) 30 min, (c) 1 h. Scare bars are 100 nm.

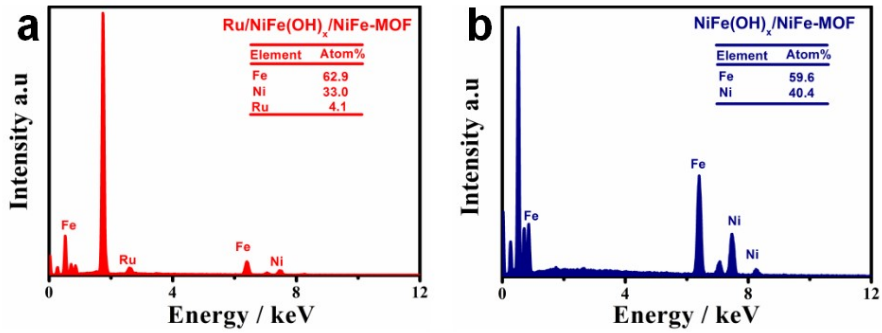

Fig.S4 EDS results of (a) Ru/NiFe(OH)$_x$/NiFe-MOF and (b) NiFe(OH)$_x$/NiFe-MOF.

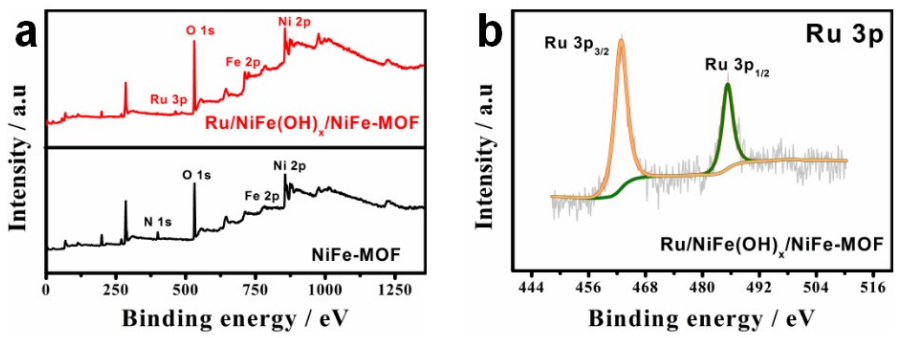

Fig.S5 (a) Survey XPS of Ru/NiFe(OH)$_x$/NiFe-MOF and NiFe(OH)$_x$/NiFe-MOF. (b) Ru 3p region of Ru/NiFe(OH)$_x$/NiFe-MOF.

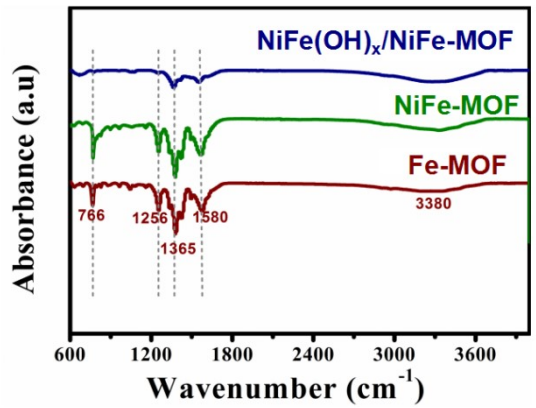

Fig.S6 FT-IR spectrum of Fe-MOF, NiFe-MOF and NiFe(OH)$_x$/NiFe-MOF.

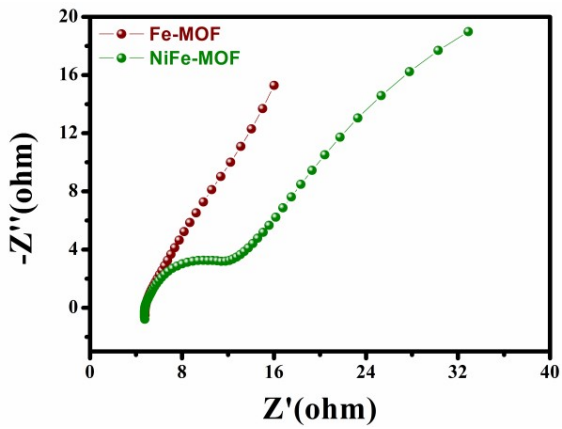

Fig.S7 EIS spectrum of Fe-MOF and NiFe-MOF.

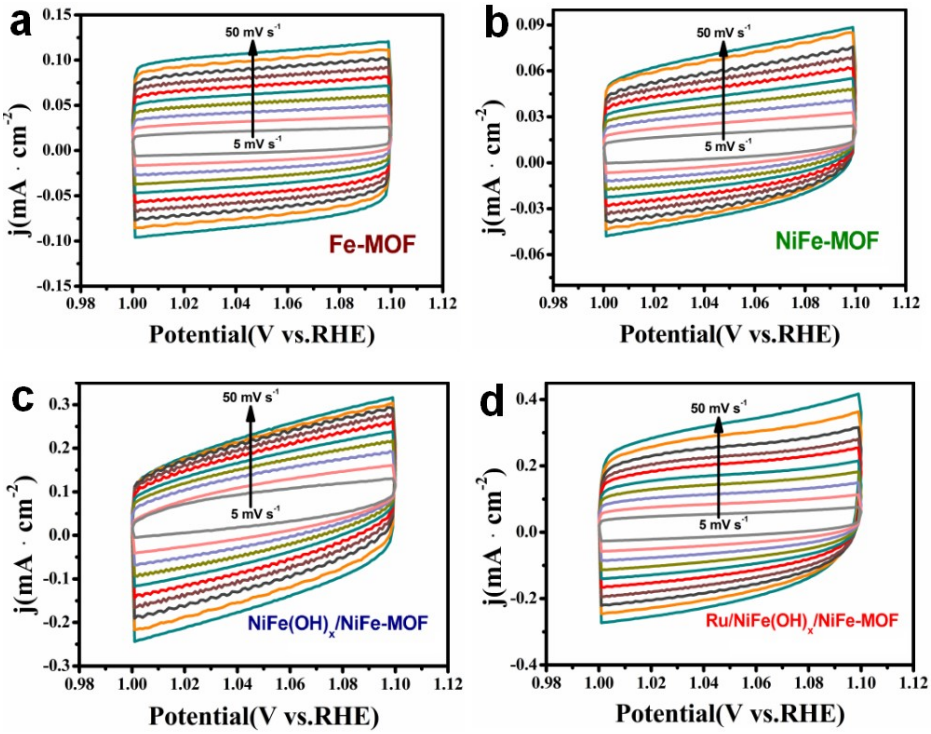

Fig.S8 CV curves of Fe-MOF, NiFe-MOF, $NiFe(OH)_x$/NiFe-MOF and Ru/$NiFe(OH)_x$/NiFe-MOF from scan rates of 5 mV s^{-1}~50 mV s^{-1}.

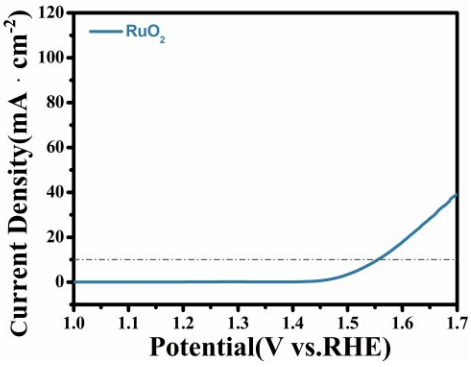

Fig.S9 LSV polarization curve of RuO_2 in 1 M KOH.

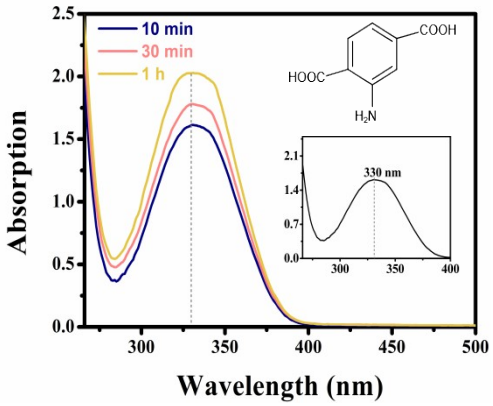

Fig.S10 UV-Vis spectroscopy of $NiFe(OH)_x$/NiFe-MOF with etching time of 10 min, 30 min and 1 h.

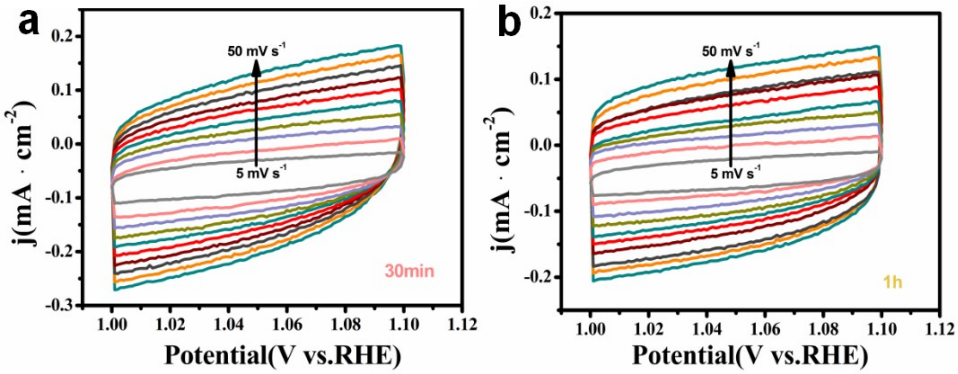

Fig.S11 CV curves of $NiFe(OH)_x$/NiFe-MOF after etching for 30 min and 1 h.

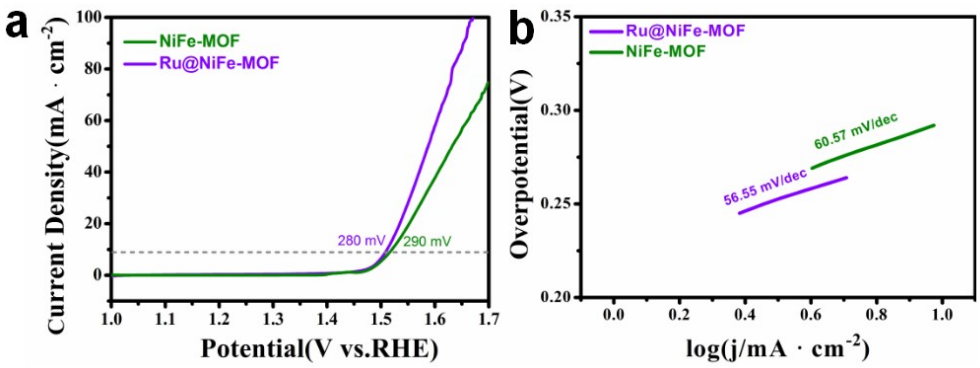

Fig.S12 (a) LSV curves of NiFe-MOF and Ru@NiFe-MOF. (b) corresponding Tafel plots.

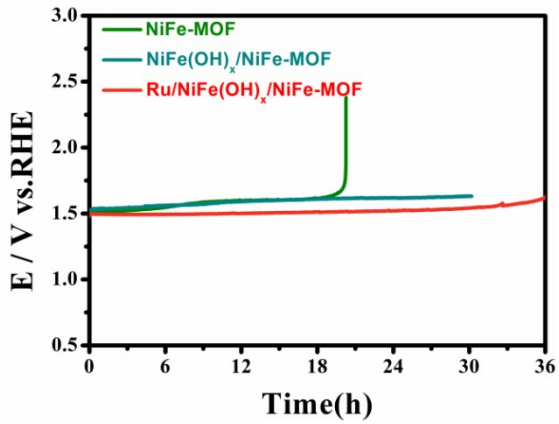

Fig.S13 Chronopotentiometric curves of Ru/NiFe(OH)$_x$/NiFe-MOF, NiFe(OH)$_x$/NiFe-MOF and NiFe-MOF at current density of 10 mA cm^{-2}.

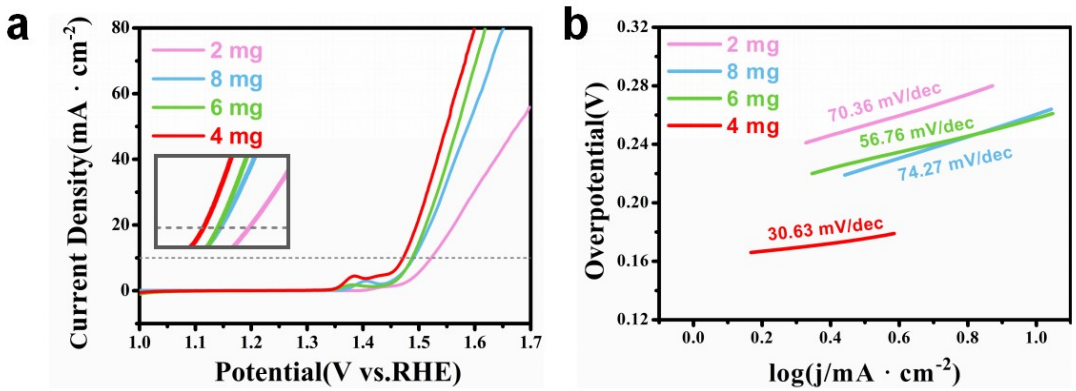

Fig.S14 (a) LSV curves of Ru/NiFe(OH)$_x$/NiFe-MOF with different amount of Ru, (b) Corresponding Tafel plots.

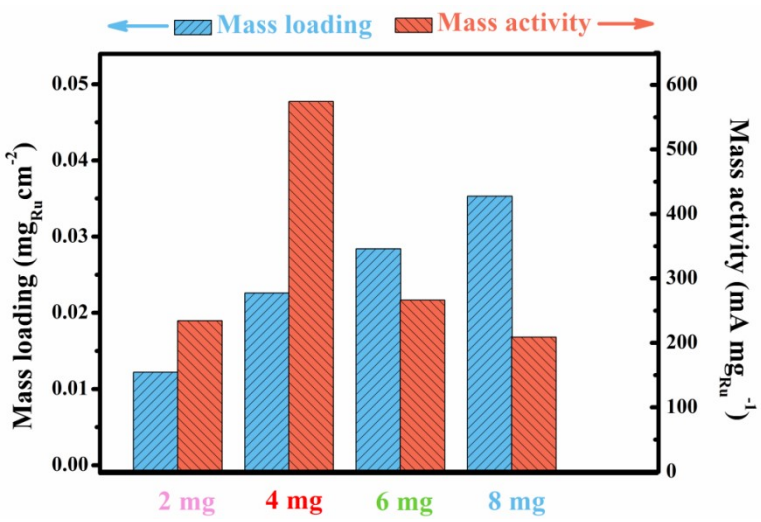

Fig.S15 Histogram of mass loading and mass activity for each sample.

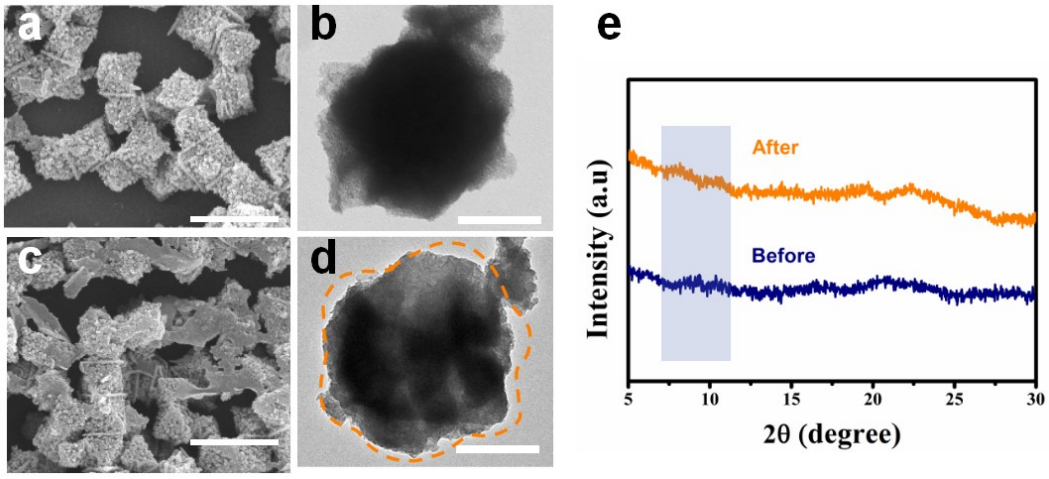

Fig.S16 SEM and TEM images of NiFe(OH)$_x$/NiFe-MOF before (a, b) and after (c, d) stability test, (e) Corresponding XRD patterns. Scale bars are 1 μm in (a, c) and 100 nm in (b, d).

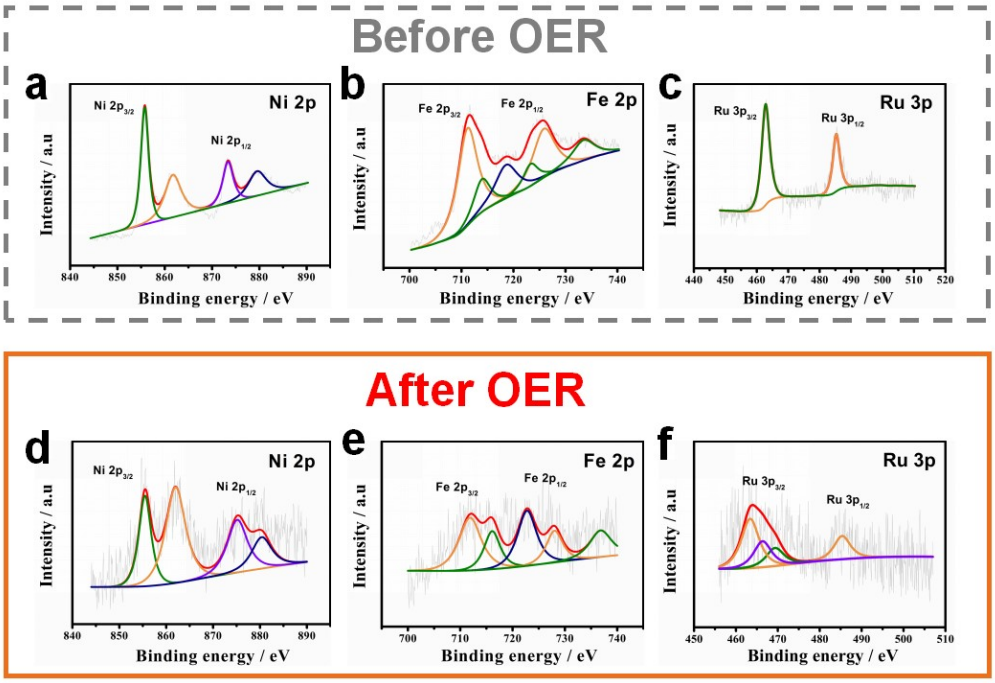

Fig.S17 XPS results of Ru/NiFe(OH)$_x$/NiFe-MOF before and after electrochemical stability test.

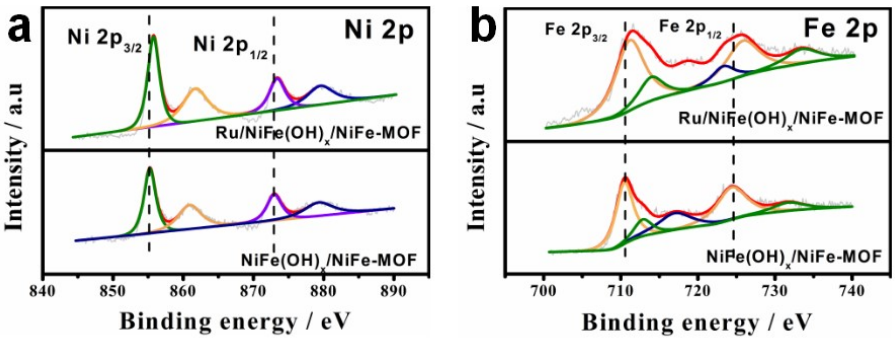

Fig.S18 The XPS results for (a) Ni 2p and (b) Fe 2p regions in Ru/NiFe(OH)$_x$/NiFe-MOF and NiFe(OH)$_x$/NiFe-MOF.

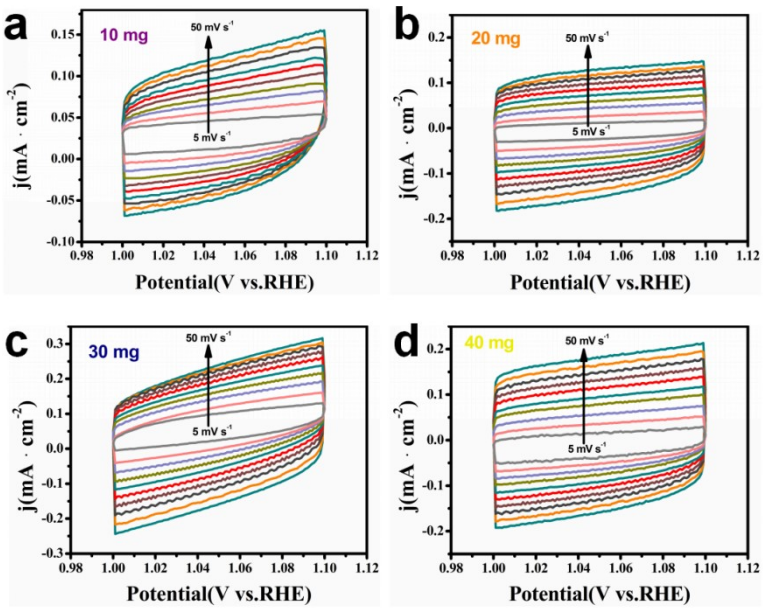

Fig.S19 CV curves of the as-fabricated $NiFe(OH)_x$/NiFe-MOF with $NiCl_2 \cdot 6H_2O$ amount of (a) 10 mg, (b) 20 mg, (c) 30 mg and (d) 40 mg respectively.

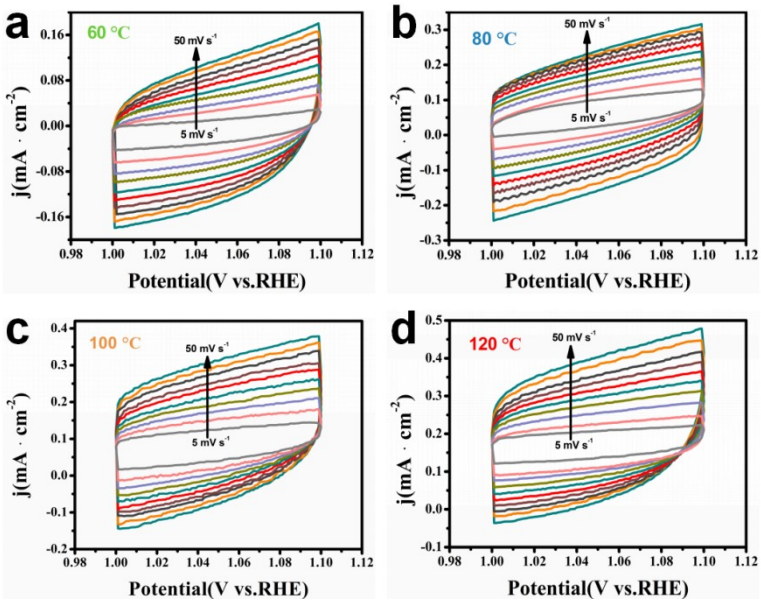

Fig.S20 CV curves of the as-fabricated $NiFe(OH)_x$/NiFe-MOF with resultant temperatures of (a) 60°C, (b) 80°C, (c) 100°C and (d) 120°C respectively.

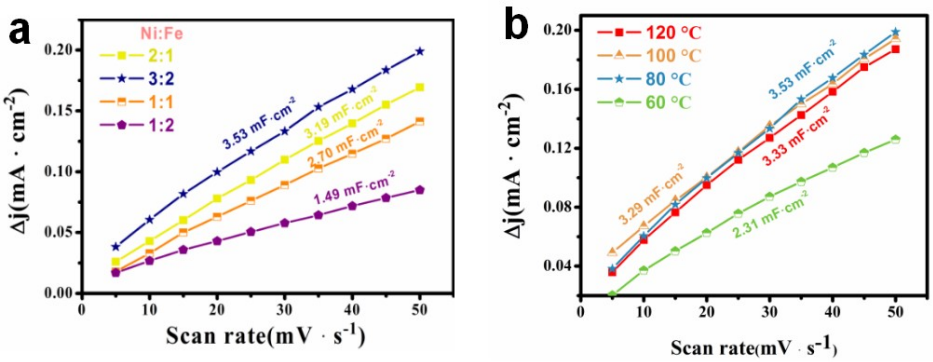

Fig.S21 Plots of current density vs. scan rate obtained by non-faradic CV scanning considering the influence of (a) proportion and (b) temperature.

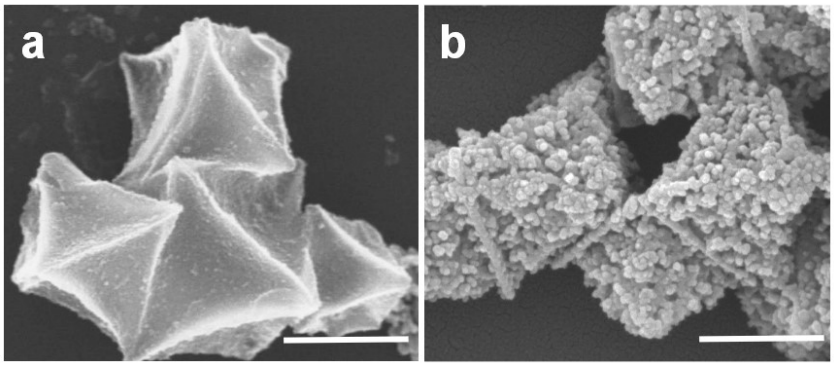

Fig.S22 SEM images of (a) NiFe-MOF and (b) $NiFe(OH)_x$/NiFe-MOF. The scale bars are 500 nm in (a) and 200 nm in (b).

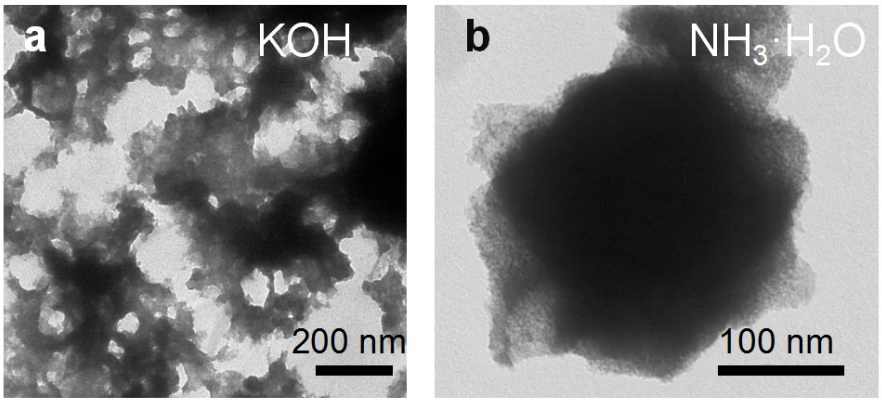

Fig.S23 TEM image of NiFe-MOF employing (a) KOH and (b) $NH_3{\cdot}H_2O$ as etching agents.

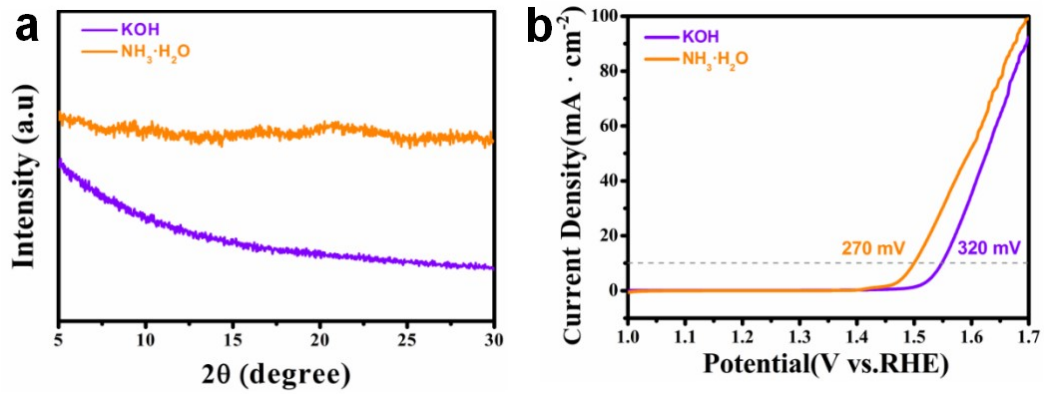

Fig.S24 (a) XRD patterns of NiFe-MOF etching by KOH (purple curve) and $NH_3 \cdot H_2O$ (orange curve) respectively, (b) LSV curves of NiFe-MOF etching by KOH and $NH_3 \cdot H_2O$ respectively.

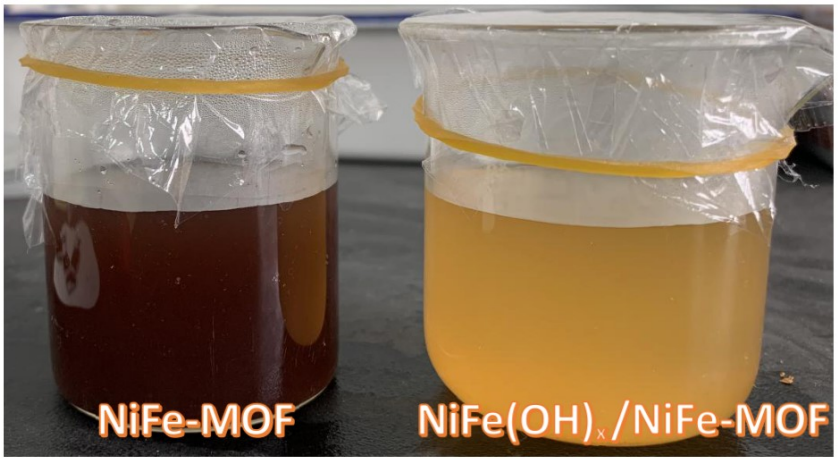

Fig.S25 Differences in colors of NiFe-MOF and $NiFe(OH)_x$/NiFe-MOF.

Table S1 Comparison of OER activity for recently reported Ru-based catalysts in alkaline condition.

Catalyst	**Overpotential (mV) at 10 mA cm^{-2}**	**Tafel slope (mV dec^{-1})**	**Reference**
Ru/NiFe(OH)$_x$/NiFe-MOF	242	30.63	This work

1-RuO_2/CeO_2	350	74	[1]
CoFeP@Ru	340	Not given	[2]
$NiCo_{1.7}Ru_{0.3}O_4$	280	78	[3]
Ru/RuO_2@N-rGO	255	44.2	[4]
$Ru(OH)_xCl_yCl$	240	75	[5]
Ru-CoMo/CFP	237	37	[6]
RuCo@NC	280	91	[7]
Ru/NiFe LDH-F/NF	230	50.2	[8]
RuRh@$(RuRh)O_2$	304	80.9	[9]
α-$Ni_{0.75}Fe_{0.25}(OH)_2$	265	54.4	[10]
FeNi-Co_3O_4	268	122.8	[11]
Ni-Fe-Se	249	36	[12]
$(FeNiCo)F_2$	260	42	[13]
FeNi SAs/NC	270	54.68	[14]
Ni-Fe-Mo film	306	77.1	[15]

Table S2 Comparison on mass activity of recently reported Ru/Ir-based electrocatalysts at 10 mA cm^{-2} in alkaline condition.

Catalyst	**Electrolyte**	**Mass activity ($mA\ mg^{-1}$)**	**η(mV at 10mA cm^{-2})**	**Reference**
$Ru/NiFe(OH)_x$/ NiFe-MOF	1.0 M KOH	574.3	250	**This work**
$Pt/NiO/RuO_2$	0.1 M $HClO_4$	~714	235	[16]

Ir_3Cu aerogel	0.1 M $HClO_4$	~400	298	[17]
$Ir_{0.7}Ru_{0.3}O_x$	0.5 M H_2SO_4	100	270	[18]
1D-RuO_2-CN_x	0.5 M H_2SO_4	352	350	[19]
IrO_2-TiO_2	0.1 M H_2SO_4	70	290	[20]
Ni@$Ru_{0.4}Co_{0.6}$	0.1 M KOH	270	330	[21]
RuO_2 NPs	0.1 M KOH	103	300	[22]
Au core-Ru	0.1 M $HClO_4$	~25	220	[23]
Ir-Ni nanoparticles	0.5 M H_2SO_4	498	280	[24]

Table S3 The mass loading of each catalysts on the electrode.

Sample	Mass $loading_{total}$ (mg cm^{-2})
Ru/NiFe$(OH)_x$/NiFe-MOF	0.229
NiFe$(OH)_x$/NiFe-MOF	0.212
NiFe-MOF	0.253
Ru@NiFe-MOF	0.236
Fe-MOF	0.258
RuO_2	0.201

Table S4 Comparison of the surface parameters, mass activity for electrocatalysts at the overpotential of 250 mV in this work.

Sample	Mass loading (mg_{Ru} cm^{-2})	Mass activity (mA mg_{Ru}^{-1})
Ru/NiFe(OH)$_x$/NiFe-MOF	0.0226	574.3
Ru@NiFe-MOF	0.0237	233.3

References

[1] Galani. S. M, Mondal. A, Srivastava. D. N and Panda. A. B, *Int. J. Hydrog. Energy*, 2020, **45**, 18635-18644.

[2] S. Liu, X. Mu, P. Ji, Y. Lv, L. Wang, Q. Zhou, C. Chen and S. Mu, *ChemCatChem*. 2020, **12**, 5149.

[3] C. Peng, H. Liu, J. Chen, Y. Zhang, L. Zhu, Q. Wu, W. Zou, J. Wang, Z. Fu and Y. Lu, *Appl. Surf. Sci*. 2021, **544**, 148897.

[4] X. Gao, J. Chen, X. Sun, B. Wu, B. Li, Z. Ning, J. Li and N. Wang, *ACS Appl. Nano Mater*. 2020, **3**, 12269-12277.

[5] W. Wang, S. Xi, Y. Shao, W. Sun, S. Wang, J. Gao, C. Mao, X. Guo, Li, G, *ACS Sustain. Chem. Eng*. 2019, **7**, 17227-17236.

[6] Y. Lin, D. Zhang and Y. Q. Gong, *Appl. Surf. Sci*. 2021, **541**, 148518.

[7] B. Sarkar, D. Das and K. K. Nanda, *Green Chem*, 2020, **22**, 7884-7895.

[8] Y. Wang, P. Zheng, M. Li, Y. Li, X. Zhang, J. Chen, X. Fang, Y. Liu, X. Yuan, X. Dai and H. Wang, *Nanoscale*, 2020, **12**, 9669-9679.

[9] K. Wang, B. Huang, W. Zhang, F. Lv, Y. Xing, W. Zhang, J. Zhou, W. Yang, F. Lin, P. Zhou, M. Li, P. Gao and S. Guo, *J. Mater. Chem. A*, 2020, **8**, 15746-15751.

[10] Y. Song, M. Song, P. Liu, W. Liu, L. Yuan, X. Hao, L. Pei, B. Xu, J. Guo and Z. Sun, *J. Mater. Chem. A*, 2021, **9**, 14372-14380.

[11] J. Li, D. Chu, D.R. Baker, A. Leff, P. Zheng and R. Jiang, *ACS Appl. Energ Mater, 2021*, DOI:10.1021/acsaem.1c01926

[12] Z. P. Wu, H. Zhang, S. Zuo, Y. Wang, S.L. Zhang, J. Zhang, S. Q. Zang and X. W. D. Lou, *Adv Mater*, 2021, e2103004.

[13] M. Nishimoto, S. Kitano, D. Kowalski, Y. Aoki and H. Habazaki, *ACS Sustain. Chem. Eng*., 2021, **9**, 9465-9473.

[14] D. Yu, Y. Ma, F. Hu, C.C. Lin, L. Li, H.Y. Chen, X. Han and S. Peng, Adv. Energy Mater., 2021, 11, 2101242.

[15] Y. Huang, Y. Wu, Z. Zhang, L. Yang and Q. Zang, Electrochim Acta, 2021, 390, 138754.

[16] Oh. A, Kim. H. Y, Baik. H, Kim. B, Chaudhari. N. K, Joo. S. H and Lee. K, *Adv. Mater*. 2019, **31**, e1805546.

[17] Q. Shi, C. Zhu, H. Zhong, D. Su, N. Li, Engelhard. M. H, H. Xia, Q. Zhang, S. Feng, Beckman. S. P, D. Du and Y. Lin, *ACS Energy. Lett*. 2018, **3**, 2038-2044.

[18] L. Wang, Saveleva. V. A, Zafeiratos. S, Savinova. E. R, Lettenmeier. P, Gazdzicki. P, Gago. A. S and Friedrich. K. A, *Nano Energy.* 2017, **34**, 385-391.

[19] Bhowmik. T, Kundu. M. K and Barman. S, *ACS Appl. Mater. Interfaces.* 2016, **8**, 28678-28688.

[20] Oakton. E, Lebedev. D, Povia. M, Abbott. D. F, Fabbri. E, Fedorov. A, Nachtegaal. M, Copéret. C and Schmidt. T. J, *ACS Catal.* 2017, **7**, 2346-2352.

[21] S. Zhang, F. Lv, X. Zhang, Y. Zhang, H. Zhu, H. Xing, Z. Mu, J. Li, S. Guo and E. Wang, *Sci. China. Mater.* 2019, **62**, 1868-1876.

[22] Nguyen. T. D, Scherer. G. G and Xu. Z. J, *Electrocatalysis.* 2016, **7**, 420-427.

[23] Gloag. L, Benedetti. T. M, Cheong. S, Y. Li, X. H. Chan, Lacroix. L. M, Chang. S. L. Y, Arenal, R, Florea. I, Barron. H, Barnard. A. S, Henning. A. M, Zhao. C, Schuhmann. W, Gooding. J. J and Tilley. R. D., *Angew. Chem. Int. Ed.* 2018, **57**, 10241-10245.

[24] J. Lim, S. Yang, C. Kim, C.-W. Roh, Y. Kwon, Y.-T. Kim, H. Lee, *Chem. Commun.* 2016, **52**, 5641-5644.